11th World Congress on Computational Mechanics (WCCM XI)
5th European Conference on Computational Mechanics (ECCM V)
6th European Conference on Computational Fluid Dynamics (ECFD VI)
E. Oñate, J. Oliver and A. Huerta (Eds)

LOW-MACH PRECONDITIONED BOUNDARY CONDITIONS FOR COMPRESSIBLE SOLVERS

J. FIEDLER AND F. DI MARE

Institute of Propulsion Technology
German Aerospace Center (DLR)
Linder Höhe
51147 Cologne
e-mail: {jens.fiedler, francesca.dimare}@dlr.de

Key Words: *low Mach precondition, compressible flows, preconditioned boundary conditions.*

Abstract. Approaching the incompressibility limit in CFD applications where compressible, density based solution methods are employed, is accompanied very often not only by slow convergence of the residuals but also by a strong degradation of the solution quality. This issue is particularly severe in turbo-machinery applications, where large variations of flow regimes occur. Low-Mach preconditioning methods can be applied to the Euler- and Navier-Stokes equations to alleviate such difficulties.

As noted by several authors, these techniques can cause stability problems especially in proximity of the domain's boundaries. In particular, it has been demonstrated that an appropriate scaling treatment is also required for characteristic-based boundary conditions.

In the current work we present the theoretical development and application of preconditioned impermeable boundaries in combination with preconditioned far-field conditions in the in-house CFD code TRACE.

1 INTRODUCTION

Preconditioning techniques based on scaling procedures have been established as an effective way of accelerating the convergence history in simulations of compressible, low-Mach flows. At low flow velocities, density-based, fully compressible solution methods can converge very slowly, or not at all, due to the large disparity between the acoustic and convective speeds. This issue can be observed in a wide range of complex technical system with locally small Mach numbers, e.g. turbomachinery configurations (cavity and seals) and low speed flow over airfoils.

Preconditioning reduces the considerable difference between the largest and smallest eigenvalue of the system's characteristic matrix. Pre-multiplication of the time derivatives by a suitable operator reduces the speed of the acoustic waves [1], hence yielding a well-conditioned system matrix. The stability of the preconditioned Euler or Navier-Stokes system of equations strongly depends on the correct treatment of the boundary conditions. Based on a preconditioning scheme previously proposed by Turkel [1] we present a consistent and stable formulation to be adopted for impermeable boundaries and its implementation in the in-house CFD code TRACE, a fully implicit parallel hybrid multi-block Reynolds-Averaged Navier-Stokes flow solver specialized in the simulation of turbo machinery flows which has been developed at DLR Cologne [12].

The validity and robustness of the method is demonstrated on an inviscid flow around a NACA0012 airfoil. It will be shown that low Mach preconditioning methods in conjunction with suitably modified boundary conditions yields an extremely fast convergence rate and strong improvement of stability at high CFL numbers. In particular, the surface pressure distribution obtained by a low Mach preconditioned calculation at very high CFL numbers ($\approx$ 100) perfectly matches the analytical solution obtained by Hejranfar et. al [9].

2 LOW-MACH PRECONDITIONED BOUNDARY CONDITIONS

Over the past decades several families of low Mach preconditioning methods, formulated using different sets of variables and satisfying different symmetry and stability requirements have been developed, as shown by Turkel [1], van Leer and Lee [2], Choi and Merkle [3], Weiss and Smith [4] and Darmofal [5]. Turkel [6] improved the artificial compressibility method which was firstly investigated by Chorin [7]. Beside the derivation of different types of preconditioning operators the study of numerical stability and the influence of modified and unmodified characteristic boundary conditions, at least for implicit schemes, remains a subject of active research. Darmofal [11] proved that an inappropriate treatment of the boundary conditions results in unphysical reflections. Because the compressible system tends to an incompressible one, it could be argued that boundary conditions developed for an incompressible scheme and described as *simplified* should already provide a physically plausible solution. We will show that the preconditioned boundary conditions developed in this work reduce to the simplified version in special cases. The numerical solution scheme used in the current work is discussed in detail in [12]. The development of the preconditioned boundary conditions is based on the characteristic variables and on the assumption of locally one-dimensional flows [8]. The characteristic variables are given by

$$W = M_U^{-1}U = \begin{pmatrix} \hat{\kappa}_x & 0 & \hat{\kappa}_z & -\hat{\kappa}_y & -\frac{\hat{\kappa}_x}{a_r^2} \\ \hat{\kappa}_y & -\hat{\kappa}_z & 0 & \hat{\kappa}_x & -\frac{\hat{\kappa}_y}{a_r^2} \\ \hat{\kappa}_z & \hat{\kappa}_y & -\hat{\kappa}_x & 0 & -\frac{\hat{\kappa}_z}{a_r^2} \\ 0 & \hat{\kappa}_x & \hat{\kappa}_y & \hat{\kappa}_z & \frac{-\hat{\lambda}'_r + \hat{a}'_r}{\beta_r^2 a_r^2 \rho_r} \\ 0 & -\hat{\kappa}_x & -\hat{\kappa}_y & -\hat{\kappa}_z & \frac{\hat{\lambda}'_r + \hat{a}'_r}{\beta_r^2 a_r^2 \rho_r} \end{pmatrix} \begin{pmatrix} \rho \\ u \\ v \\ w \\ p \end{pmatrix} \tag{1}$$

where M^{-1} is the inverse eigenvector matrix obtained as a result of the matrix decomposition of the stabilization term of the modified Roe scheme. The quantities *ρ, u, v, w, p* and *a* are the density, velocity components, pressure and sound speed, respectively. The variable β is the preconditioning parameter depending on local flow conditions. Extensive studies have been performed on the influence of β on the numerical stability of a preconditioned system, e.g. [13]. Often, β is determined by the local Mach number and limited by a heuristic cut-off value. In the current work all boundary conditions used by the presented testcase have been consistently modified. Therefore, β is related to the local Mach number and bounded above by *1*. The preconditioned sound speed $\hat{a}'_r$ and eigenvalue $\hat{\lambda}'_r$ are given by

$$\begin{aligned} \hat{a}'_r &= \frac{1}{2}\sqrt{(1-\beta_r^2)^2\hat{\lambda}_r^2 + 4\beta_r^2 a_r^2} \\ \hat{\lambda}'_r &= \frac{1-\beta^2}{2}\hat{\lambda}_r \\ \hat{\lambda}_r &= \hat{\kappa}_x u_r + \hat{\kappa}_y v_r + \hat{\kappa}_z w_r \end{aligned} \tag{2}$$

The components of the metric vector have been normalized by

$$\hat{\kappa}_i = \kappa_i / \|\kappa\| \tag{3}$$

This yields:

$$\hat{\lambda}_i = \lambda_i / \|\kappa\| \tag{4}$$

By carrying out the product in (1) one obtains:

$$\begin{aligned} W_1 &= \hat{\kappa}_x\rho + \hat{\kappa}_z v - \hat{\kappa}_y w - \frac{\hat{\kappa}_x}{a_r^2}p \\ W_2 &= \hat{\kappa}_y\rho - \hat{\kappa}_z u - \hat{\kappa}_x w - \frac{\hat{\kappa}_y}{a_r^2}p \\ W_3 &= \hat{\kappa}_z\rho + \hat{\kappa}_y u - \hat{\kappa}_x v - \frac{\hat{\kappa}_z}{a_r^2}p \end{aligned} \tag{5}$$

$$W_4 = \hat{\kappa}_x u + \hat{\kappa}_y v + \hat{\kappa}_z w + \frac{-\hat{\lambda}'_r + \hat{a}'_r}{\beta_r^2 a_r^2 \rho_r} p$$
$$W_5 = -\hat{\kappa}_x u - \hat{\kappa}_y v - \hat{\kappa}_z w + \frac{\hat{\lambda}'_r + \hat{a}'_r}{\beta_r^2 a_r^2 \rho_r} p$$

Each eigenvalue is associated with a particular characteristic variable and indicates the direction of propagation of the information they contain. Referring to fig. (1), an inflow is determined by the condition $\boldsymbol{v} \cdot \boldsymbol{n} < 0$. Hence, the first three and fifth eigenvalue are negative whilst the fourth is positive. Four characteristic variables must be therefore specified and one is determined from the information inside the domain. The subscript r refers to reference values, which can be taken at the center of the first interior cell adjacent to the boundary.

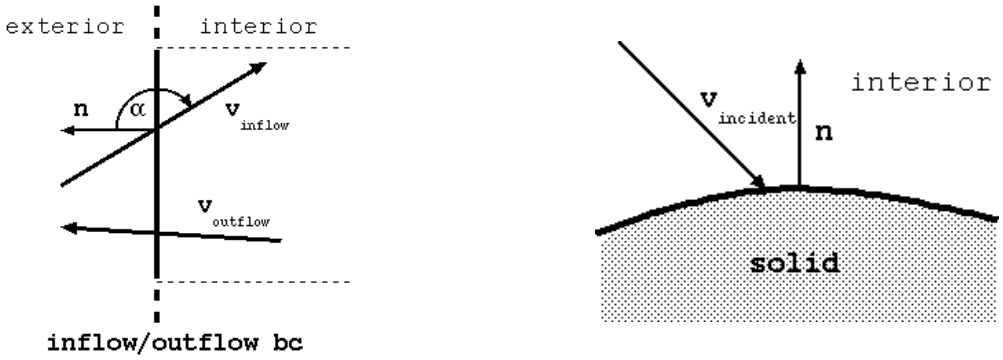

Figure 1: Orientation of the face normal vector used for different types of boundaries.

2.1 Far-field boundary conditions

The system of equations to determine the far-field boundary conditions is given by

$$\begin{aligned}
\left(\hat{\kappa}_x \rho + \hat{\kappa}_z v - \hat{\kappa}_y w - \frac{\hat{\kappa}_x}{a_r^2} p\right)_b &= \left(\hat{\kappa}_x \rho + \hat{\kappa}_z v - \hat{\kappa}_y w - \frac{\hat{\kappa}_x}{a_r^2} p\right)_{c1} \\
\left(\hat{\kappa}_y \rho - \hat{\kappa}_z u - \hat{\kappa}_x w - \frac{\hat{\kappa}_y}{a_r^2} p\right)_b &= \left(\hat{\kappa}_y \rho - \hat{\kappa}_z u - \hat{\kappa}_x w - \frac{\hat{\kappa}_y}{a_r^2} p\right)_{c2} \\
\left(\hat{\kappa}_z \rho + \hat{\kappa}_y u - \hat{\kappa}_x v - \frac{\hat{\kappa}_z}{a_r^2} p\right)_b &= \left(\hat{\kappa}_z \rho + \hat{\kappa}_y u - \hat{\kappa}_x v - \frac{\hat{\kappa}_z}{a_r^2} p\right)_{c3} \\
\left(\left(\hat{\kappa}_x u + \hat{\kappa}_y v + \hat{\kappa}_z w\right) + \frac{-\hat{\lambda}'_r + \hat{a}'_r}{\beta_r^2 a_r^2 \rho_r} p\right)_b &= \left(\left(\hat{\kappa}_x u + \hat{\kappa}_y v + \hat{\kappa}_z w\right) + \frac{-\hat{\lambda}'_r + \hat{a}'_r}{\beta_r^2 a_r^2 \rho_r} p\right)_{c4} \\
\left(-\left(\hat{\kappa}_x u + \hat{\kappa}_y v + \hat{\kappa}_z w\right) + \frac{\hat{\lambda}'_r + \hat{a}'_r}{\beta_r^2 a_r^2 \rho_r} p\right)_b &= \left(-\left(\hat{\kappa}_x u + \hat{\kappa}_y v + \hat{\kappa}_z w\right) + \frac{\hat{\lambda}'_r + \hat{a}'_r}{\beta_r^2 a_r^2 \rho_r} p\right)_{c5}
\end{aligned} \tag{6}$$

where $c_1, \ldots, c_5$ are properties to be specified depending on whether the flows enters or leaves the domain. At a subsonic inflow c_1, c_2, c_3, c_5 have to be determined through quantities specified at infinity and indicated by the subscript ∞ and c_4 is extrapolated from the interior, where the subscript i is used. At a subsonic outflow c_1, c_2, c_3, c_5 are determined using interior

values and c_4 must be specified. The last two relations of (6) can be combined to give [9]

$$\begin{aligned} p_b &= p_\infty + \left(1 - \frac{\hat{\lambda}'_r}{\hat{a}'_r}\right)\left(\frac{p_r - p_\infty}{2}\right) + \frac{\rho_r \beta_r^2 a_r^2}{\hat{a}'_r}\left(\frac{\hat{\lambda}_r - \hat{\lambda}_\infty}{2}\right) \\ \hat{\lambda}_b &= \hat{\lambda}_r - \left(1 - \frac{\hat{\lambda}'_r}{\hat{a}'_r}\right)\left(\frac{\hat{\lambda}_r - \hat{\lambda}_\infty}{2}\right) + \frac{1}{\rho \hat{a}'_r}\left(\frac{p_r - p_\infty}{2}\right) \end{aligned} \tag{7}$$

and can be consistently used at both inflow and outflow boundaries. The velocity components at an inflow are given by [9]

$$\begin{aligned} u_b &= u_\infty + \hat{\kappa}_x\left(\hat{\lambda}_b - \hat{\lambda}_\infty\right) \\ v_b &= v_\infty + \hat{\kappa}_y\left(\hat{\lambda}_b - \hat{\lambda}_\infty\right) \\ w_b &= w_\infty + \hat{\kappa}_z\left(\hat{\lambda}_b - \hat{\lambda}_\infty\right) \end{aligned} \tag{8}$$

Invoking the assumption that the flow is isentropic, a relation for the density can be derived. Using

$$S_b = S_\infty \tag{9}$$

one obtains

$$\rho_b = \rho_\infty \left(\frac{p_b}{p_\infty}\right)^{1/\gamma} \tag{10}$$

The velocity components at an outflow boundary read [9]

$$\begin{aligned} u_b &= u_i + \hat{\kappa}_x\left(\hat{\lambda}_b - \hat{\lambda}_i\right) \\ v_b &= v_i + \hat{\kappa}_y\left(\hat{\lambda}_b - \hat{\lambda}_i\right) \\ w_b &= w_i + \hat{\kappa}_z\left(\hat{\lambda}_b - \hat{\lambda}_i\right) \end{aligned} \tag{11}$$

and similar to (10) the density is

$$\rho_b = \rho_i \left(\frac{p_b}{p_i}\right)^{1/\gamma} \tag{12}$$

All other physical quantities can be derived from the above relationships.

2.2 Impermeable boundary conditions

For the determination of the state variables at impermeable walls, the following relations among the characteristic variables based on (5) have been used [8]:

$$\begin{gathered}
\left(\hat{\kappa}_x\rho + \hat{\kappa}_z v - \hat{\kappa}_y w - \frac{\hat{\kappa}_x}{a_r^2}p\right)_b = \left(\hat{\kappa}_x\rho + \hat{\kappa}_z v - \hat{\kappa}_y w - \frac{\hat{\kappa}_x}{a_r^2}p\right)_r \\
\left(\hat{\kappa}_y\rho - \hat{\kappa}_z u - \hat{\kappa}_x w - \frac{\hat{\kappa}_y}{a_r^2}p\right)_b = \left(\hat{\kappa}_y\rho - \hat{\kappa}_z u - \hat{\kappa}_x w - \frac{\hat{\kappa}_y}{a_r^2}p\right)_r \\
\left(\hat{\kappa}_z\rho + \hat{\kappa}_y u - \hat{\kappa}_x v - \frac{\hat{\kappa}_z}{a_r^2}p\right)_b = \left(\hat{\kappa}_z\rho + \hat{\kappa}_y u - \hat{\kappa}_x v - \frac{\hat{\kappa}_z}{a_r^2}p\right)_r \\
\left(\hat{\kappa}_x u + \hat{\kappa}_y v + \hat{\kappa}_z w\right)_b = 0 \\
\left(\left(\hat{\kappa}_x u + \hat{\kappa}_y v + \hat{\kappa}_z w\right) + \frac{\hat{\lambda}'_r + \hat{a}'_r}{\beta_r^2 a_r^2 \rho_r}p\right)_b = \left(\left(\hat{\kappa}_x u + \hat{\kappa}_y v + \hat{\kappa}_z w\right) + \frac{\hat{\lambda}'_r + \hat{a}'_r}{\beta_r^2 a_r^2 \rho_r}p\right)_r
\end{gathered} \tag{13}$$

The fourth relation corresponds to the condition that there is no flow across the boundary. As also reported in [8] the sign of the fifth equality in (13) accounts for the orientation of the normal at impermeable boundaries (as shown in fig. (1)). The last two relations of (13) can be then solved for p_b. This yields:

$$p_b = p_r + \frac{\beta_r^2 a_r^2 \rho_r}{\hat{a}'_r + \hat{\lambda}'_r}\hat{\lambda}_r \tag{14}$$

The first four relations are used to obtain the remaining four variables. The result read:

$$\begin{aligned}
u_b &= u_r - \hat{\kappa}_x\hat{\lambda}_r \\
v_b &= v_r - \hat{\kappa}_y\hat{\lambda}_r \\
w_b &= w_r - \hat{\kappa}_z\hat{\lambda}_r \\
\rho_b &= \rho_r + \frac{p_b - p_r}{a_r^2}
\end{aligned} \tag{15}$$

It is worth mentioning that the original formulation of Whitfield and Janus [8] is recovered for $\beta = 1$.

2.3 Simplified boundary conditions

At low Mach numbers the compressible system tends to the incompressible one. In this case in- and outflow conditions employed for incompressible regimes should already provide physically realistic solutions. It can be shown that the *simplified* far-field boundary conditions are indeed a special case of those derived in the previous sections. At a subsonic inflow, one has, in particular [9, 10]

$$p_b = p_i, u_b = u_\infty, v_b = v_\infty, w_b = w_\infty, \rho_b = \rho_\infty \tag{16}$$

and at a subsonic outflow

$$p_b = p_\infty, u_b = u_i, v_b = v_i, w_b = w_i, \rho_b = \rho_i \tag{17}$$

The accuracy of this type of boundary conditions is examined in the following section by comparison with the fully consistent one derived in this work.

3 NUMERICAL METHOD

All calculations have been performed using the in-house CFD code TRACE. This is a fully implicit, parallel, hybrid multi-block Reynolds-Averaged Navier-Stokes flow solver specialized in the simulation of turbo machinery flows which has been developed at DLR Cologne [14].

The three-dimensional Navier-Stokes equations in a rotating frame of reference are solved using the finite volume approach, with the convective fluxes being discretized by means of Roe's flux difference splitting scheme [15]. In the case of steady computations TRACE uses a time-marching method, whilst for unsteady solutions a dual-time stepping procedure is adopted [16], where the physical time derivatives are used to march the unsteady equations whereas the pseudo-time derivatives are used for purposes of numerical iteration. In order to maintain the temporal accuracy of the scheme, only the pseudo-time iterations are affected by the preconditioning.

4 RESULTS

The inviscid flow around the NACA0012 airfoil at an angle of attack of 5° has been investigated to prove the stability and accuracy of the boundary treatment developed in the current work. The free stream Mach number is set to $M_{\infty} = 0.01$. The far-field radius is given by $R = 5c$, where R is the radius of the far-field boundary (distance of the leftmost grid point of the far-field boundary from the leading edge of the airfoil) and c the airfoil chord length. The calculations have been performed using a symmetric Gauss Seidel solution procedure. Details are discussed in [12]. The computational domain is decomposed into two blocks of mesh sizes 288 x 71 and 112 x 144 nodes and is shown in fig. (3).

A grid independency study has also been carried out and four grids have been generated by successive refinement. In order to show the grid independency of the converged solution, the normalised integrated surface pressure coefficient has been identified as sensitive grid parameter and shown in fig. (2).

In the current configuration the CFL number has been set equal to 100. From the convergence rate observed by the preconditioned computations, fig. (5), it can be seen that already approx. 1500 iterations are sufficient to reduce the residuals down to machine precision. Compared to the work of [9] the current convergence history is strongly accelerated. The predicted Cp distribution, shown in fig. (8), is also in perfect agreement with results published by [9], which were obtained using the panel method. A consistent boundary treatment suppresses the appearance of unphysical reflections in the proximity of boundaries. This is shown on the smooth distribution of the isolines of β, presented in fig. (7), which also confirms the numerical stability of the scheme in the whole computational domain. It also apparent, that a consistent formulation of the boundary conditions provides best results in both quality and convergence acceleration. In principle this suggests that no particular cut-off value for the preconditioned parameter β is required to stabilize the preconditioning scheme. Moreover, it can be seen that simulations of flows with low convective speeds carried out using high CFL number with no low-Mach preconditioning do not automatically result in improvement of the convergence history and quality of solution, (figs. (4) and (8)). For comparison, further calculations have been performed using *simplified* boundary conditions previously developed for purely incompressible flows [9, 10]. The results are shown in figs.

(6) and (8) and confirm that an acceptable quality in results and convergence speed can be reached, which however is inferior to those obtained using a fully consistent treatment.

5 CONCLUSIONS

The numerical stability of low-Mach preconditioned scheme is strongly influenced by the boundary treatment. In this study a novel formulation of the impermeable boundary conditions low-Mach preconditioned has been derived and its successful implementation in a full-implicit three-dimensional compressible Navier-Stokes flow solver demonstrated. In conjunction with appropriately modified far-field conditions recently published in literature [9] excellent results have been obtained, particularly with regards to convergence acceleration also at very high CFL number (≈ 100) and improvement in the overall quality of the results. The validity of the method has been demonstrated in a series of numerical simulations of the inviscid flow around a NACA0012 airfoil profile. For completeness *simplified* boundary conditions that are derived for strictly incompressible flows have also been considered and it has been confirmed that they do results of acceptable quality, although at the expense of flexibility.

REFERENCES

[1] Turkel, E. Preconditioning techniques in computational fluid dynamics. *Annu. Rev. Fluid. Mech.* (1999) **31**:385-416

[2] van Leer, B., Lee, W.-T. and Roe, P. L. Characteristic time-stepping or local preconditioning of the Euler equations. *10th Computational Fluid Dynamics Conference* (1991)

[3] Choi, Y.-H. and Merkle, C. L. The application of preconditioning in viscous flows. *J. Comput. Phys.* (1993) **105**:207-223

[4] Weiss, J. M. and W. A. Smith, W. A. Preconditioning applied to variable and constant density flows. *AIAA Journal* (1995) **33**:2050-2057

[5] Darmofal, D. L. and van Leer, B. Local preconditioning of the Euler equations: A characteristic interpretation.

[6] Turkel, E. Preconditioned methods for solving the incompressible low speed compressible equations. *J. Comput. Phys.* (1987) **72**:277-298

[7] Chorin, A. J. A numerical method for solving incompressible viscous flow problems. *J. Comput. Phys.* (1967) **2**:12-26

[8] Whitfield, D. L. and Janus, J. M. Three-dimensional unsteady Euler equations solution using flux vector splitting. *AIAA-84-1552* (1984)

[9] Hejranfar, K and Kamali-Moghadam, R. Preconditioned characteristic boundary conditions for solution of the preconditioned Euler equations at low Mach number flows. *J. Comput. Phys.* (2012) **12**:4384-4402

[10] Turkel, E., Vatsa, V. N. and Radespiel, R. Preconditioning methods for low-speed flows. *NASA/CR-1996-201605* (1996)

[11] Darmofal, D. L. Eigenmode analysis of boundary conditions for the one-dimensional preconditioned Euler equations. *NASA/CR-1998-208741* (1998)

[12] Fiedler, J. and di Mare, F. Generalised implementation of low-Mach preconditioning for arbitrary three-dimensional geometries. *Proceedings of the 6th European Congress on Computational Methods in Applied Science and Engineering* (ECCOMAS 2012), Vienna, Austria, Sept. 2012.

[13] Colin, Y., Deniau, H. and Boussuge, J.-F. A robust low speed preconditioning formulation for viscous flow computations. *Comput. Fluids* (2011) **47**:1-15

[14] Becker, K., Heitkamp, K. and Kügeler, E. Recent progress in a hybrid-grid CFD solver for turbomachinery flows. *Proceedings of the 5th European Congress on Computational Methods in Applied Science and Engineering* (ECCOMAS 2010), Lisbon, Portugal, June (2010)

[15] Roe, P. L. Approximate Riemann solvers, parameter vectors and difference schemes. *J. Comp. Phys.* (1981) **43**:357-372

[16] Pandya, S. A., Venkateswaran, S. and Pulliam, T. H. Implementation of preconditioned dual-time procedures in OVERFLOW. *AIAA 2003-0071* (2003).

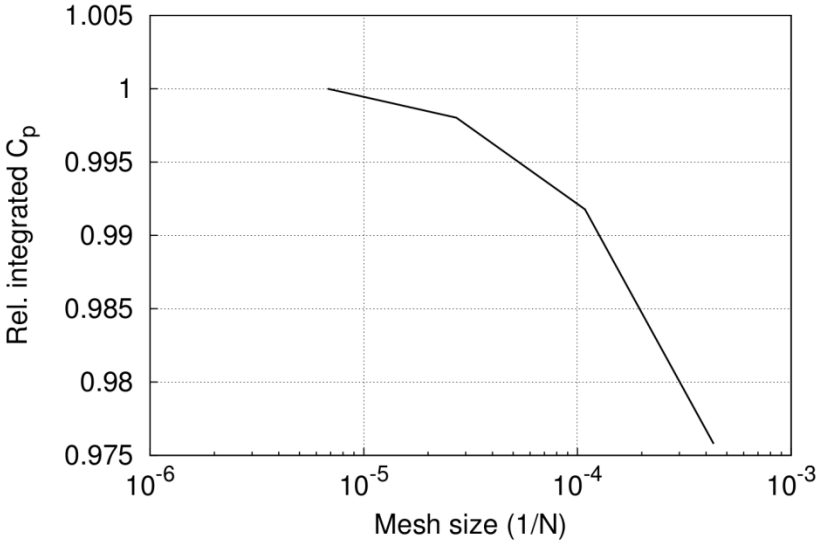

Figure 2: Grid convergence based on the integrated and normalized surface pressure coefficient.

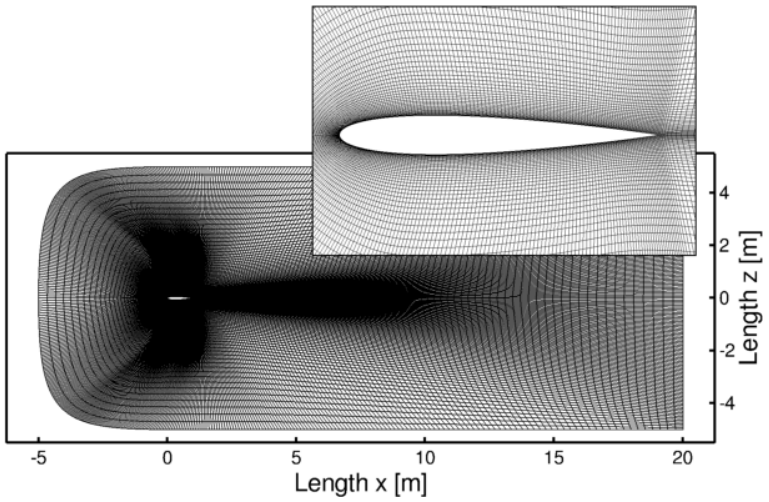

Figure 3: General setup of a NACA0012 airfoil profile.

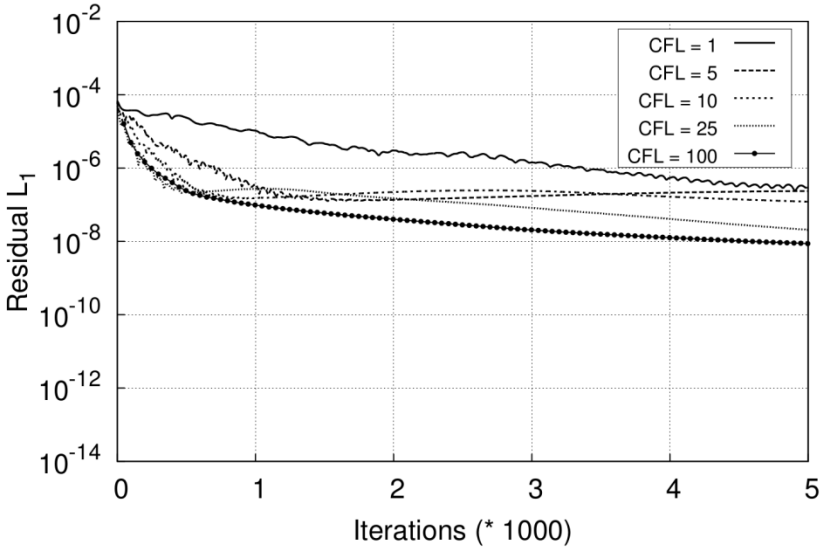

Figure 4: L_1 Residual at increasing CFL number for reference calculations.

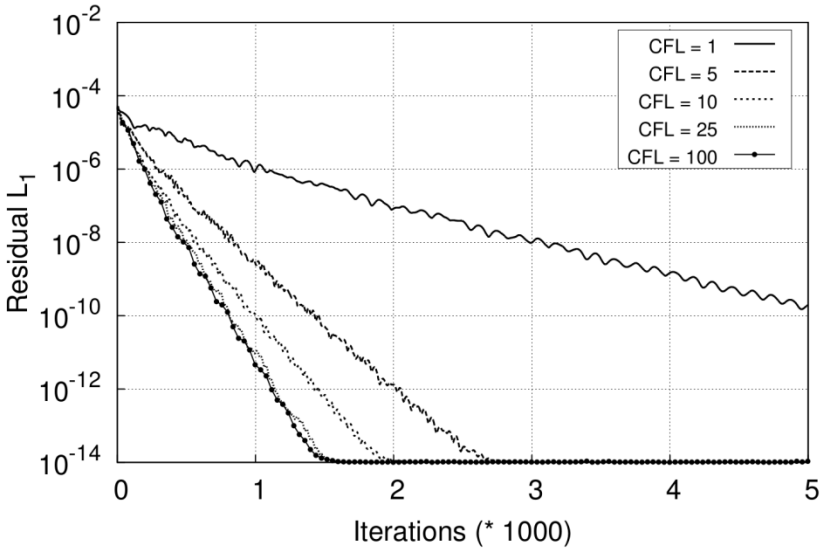

Figure 5: L_1 Residual at increasing CFL number for computations taking a consistent formulation of the preconditioned far-field and impermeable boundary conditions into account.

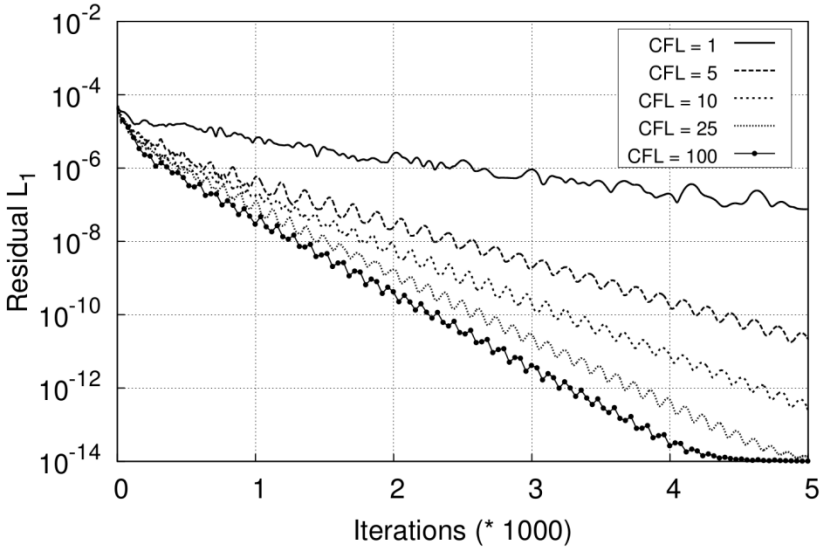

Figure 6: L_1 Residual at increasing CFL number for the computation taking a simplified formulation of the far-field boundary conditions into account.

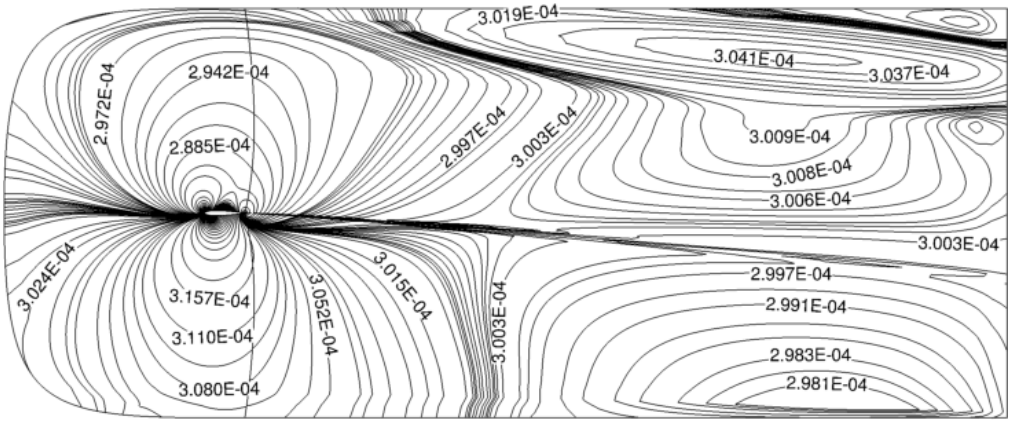

Figure 7: Isolines of β^2 within the far-field region.

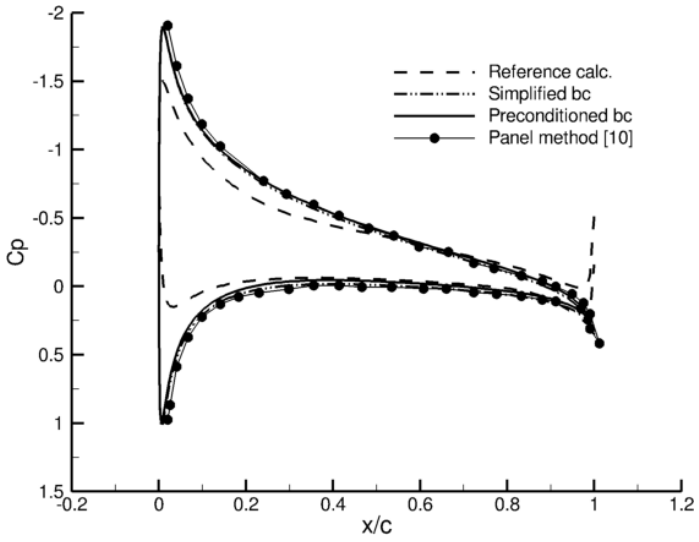

Figure 8: Cp distribution around a NACA0012 airfoil for non-preconditioned (Reference) and preconditioned calculations using consistent far-field and simplified conditions.